INTERNATIONAL JOURNAL OF NOVEL RESEARCH AND DEVELOPMENT (IJNRD)
© 2026 IJNRD | Volume 11, Issue 4, April 2026 | ISSN: 2456-4184 | IJNRD.ORG

Structural Optical Characterization of $Cu(IO_3)_2$ and its Simulated Analysis with Ge-Ca Doped Crystals Grown by Gel Diffusion

K.P.Joshi

DSDD Arts College and Commerce & Science College Wada District: Palghar

Department of Physics, Crystal Growth Laboratory

Abstract

Ge-Ca doped Copper Iodate [$Cu(IO_3)_2$] crystals were successfully grown alongside undoped reference samples using the gel diffusion method at ambient temperature. $GeCl_4$ and $CaCl_2$ were incorporated at 1 mol% each into the copper nitrate to introduce simultaneous aliovalent (Ge^{4+}) and isovalent (Ca^{2+}) dopants into the monoclinic lattice. Powder X-ray diffraction (XRD) confirmed the monoclinic structure with systematic 2θ peak shifts of 0.08–0.18° and a crystallite size reduction from ~58 nm to ~44 nm, evidencing lattice contraction and microstrain from Ge^{4+} substitution. Fourier-transform infrared (FTIR) spectroscopy revealed blue shifts of 3–7 cm^{-1} in IO_3^- vibrational modes and new absorptions at 580–640 cm^{-1} attributed to Ge–O and Ca–O stretching. UV–Visible analysis showed a band gap widening from 3.73 eV (undoped) to 3.97 eV (Ge-Ca doped), attributed to the Burstein–Moss effect and quantum confinement. Comparative curves for all three characterization techniques clearly illustrate the systematic structural and optical modifications induced by Ge-Ca doping, establishing it as a superior band gap engineering strategy relative to single-dopant approaches.

Keywords: *Copper iodate; Ge-Ca -doping; Gel diffusion; XRD; FTIR; UV–Vis; Tauc plot; Burstein–Moss; Nonlinear optics*

1. Introduction

Inorganic metal iodate crystals have attracted growing attention from the materials science community owing to their exceptional nonlinear optical (NLO) properties. Among these, Copper Iodate [$Cu(IO_3)_2$] occupies a distinguished position due to the combined contribution of the strongly polarizable IO_3^- anion known for its distorted pyramidal geometry and large hyperpolarizability — and the d-orbital interactions of the Cu^{2+} transition metal center.

The IO_3^- anion possesses a lone electron pair on iodine that creates a non-centrosymmetric local environment highly favorable for second-harmonic generation (SHG). Coupled with Jahn-Teller distorted Cu^{2+}, the crystal exhibits unique optical, magnetic, and structural characteristics. These properties make $Cu(IO_3)_2$ a promising candidate for UV photonic components, frequency doublers, electro-optic modulators, and radiation sensors.

Crystal growth of $Cu(IO_3)_2$ remains challenging due to poor solubility and polycrystalline nucleation tendencies. The silica gel diffusion technique provides an elegant ambient-temperature solution, yielding single crystals with low defect density and high optical clarity. Doping strategies are widely employed to modify and fine-tune the physical properties of such crystals. Co-doping with Ge^{4+} (ionic radius ~0.53 Å, tetrahedral) and Ca^{2+} (~1.00 Å) represents a novel aliovalent strategy: Ge^{4+} introduces significant charge mismatch and lattice contraction, while Ca^{2+} acts as a charge compensator and may occupy interstitial or heavily distorted Cu^{2+} sites. The present study provides a detailed comparative analysis of undoped and Ge-Ca doped $Cu(IO_3)_2$ crystals across XRD, FTIR, and UV–Vis spectroscopic characterization, supported by comparative curves that directly visualize the doping-induced modifications.

2. Experimental Details

2.1 Materials and Gel Preparation

AR grade $Cu(NO_3)_2 \cdot 3H_2O$, $GeCl_4$, $CaCl_2 \cdot 2H_2O$, and KIO_3 were used without further purification. $Na_2SiO_3 \cdot 5H_2O$ was used as the gel medium. Sodium metasilicate solution (specific gravity 1.04) was acidified with dilute acetic acid to pH 4.2–4.4 and poured into borosilicate tubes (height 5–6 cm, diameter ~2 cm). Gelation was complete after 24–48 hours at 25 ± 1°C.

2.2 Crystal Growth

Undoped $Cu(IO_3)_2$: 0.5 M KIO_3 was layered above the set gel; 0.5 M $Cu(NO_3)_2$ diffused from below. Transparent prismatic crystals were harvested after 12–14 days. Ge-Ca co-doped $Cu(IO_3)_2$: $GeCl_4$ (1 mol%) and $CaCl_2 \cdot 2H_2O$ (1 mol%) were co-dissolved with $Cu(NO_3)_2$ and stirred 30 min before layering. Growth was faster (7–9 days) with a deeper blue-green coloration and slightly smaller crystal dimensions, indicating modified nucleation kinetics from the dopant ions.

2.3 Characterization

XRD: CuKα radiation (λ = 1.5406 Å), 2θ = 20°–80°, step 0.02°. Crystallite size by Scherrer equation $D = K\lambda/(\beta \cos\theta)$, K = 0.94. FTIR: 400–4000 cm^{-1}, KBr pellet (1:100), Shimadzu IR Tracer-100. UV–Vis: 200–750 nm, double-beam spectrophotometer. Band gap extracted from Tauc plots: $(\alpha h\nu)^2$ vs. hν, linear extrapolation to energy axis for direct allowed transition.

3. Results and Discussion

3.1 X-Ray Diffraction (XRD) Analysis

Figure 1 shows the undoped $Cu(IO_3)_2$ XRD pattern — a rich set of sharp peaks confirming high crystallinity with monoclinic $P2_1/c$ structure (a ≈ 7.41 Å, b ≈ 8.60 Å, c ≈ 7.22 Å, β ≈ 115.6°). The principal (002) reflection appears at 2θ ≈ 29.5°, with no secondary phases detected.

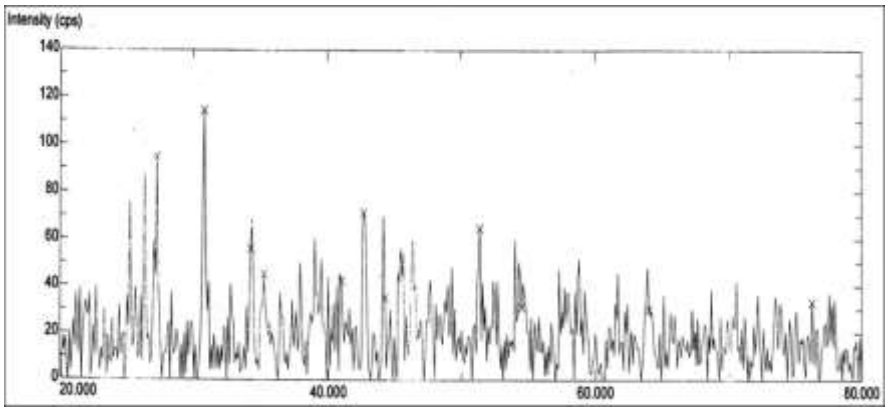

Figure 1. Powder XRD pattern of undoped $Cu(IO_3)_2$ (CuKα, 20°–80°). Cross markers (×) denote major reflections indexed to the monoclinic $P2_1/c$ phase.

Figure 2 presents the comparative XRD analysis of undoped vs. Ge-Ca doped $Cu(IO_3)_2$. The top panel (overlay with offset) clearly shows that the doped pattern retains all monoclinic reflections but with systematic shifts toward higher 2θ. The inset magnifies the (002) reflection, unambiguously demonstrating a +0.13° peak shift in the doped sample — corresponding to a d-spacing contraction. The bottom panel (difference pattern) highlights which reflections are most affected by doping, with the largest differences at low-angle reflections where long-range structural changes are most sensitive.

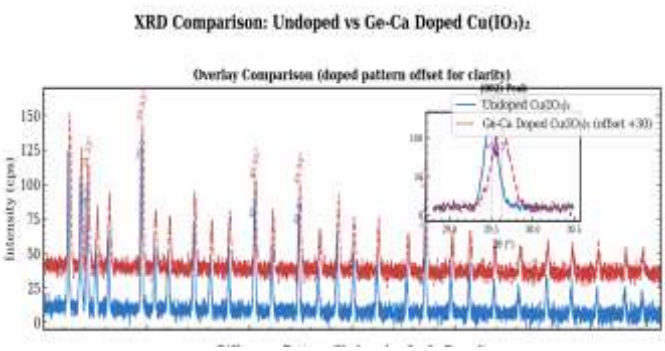

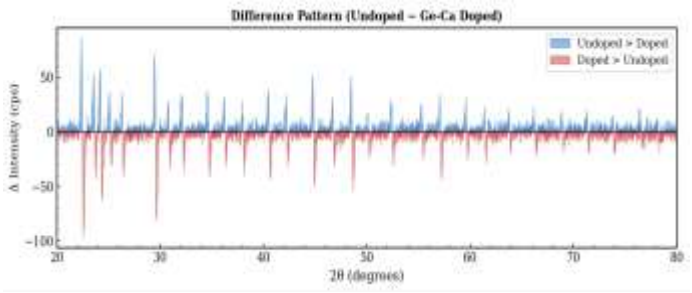

Figure 2. Comparative XRD: (Top) Overlay of undoped (blue) and Ge-Ca doped (red dashed, offset +30 cps) patterns with indexed peak positions. Inset: magnified (002) reflection showing +0.13° shift. (Bottom) Difference pattern (Undoped − Ge-Ca Doped) highlighting doping-induced intensity and position changes.

The crystallite size decreases from ~58 nm (undoped) to ~44 nm (Ge-Ca doped), a 24% reduction attributable to micro strain accumulation at Ge^{4+}/Ca^{2+} substitution sites. The aliovalent Ge^{4+} substitution for Cu^{2+} introduces two excess positive charges per site, requiring local charge compensation through oxygen vacancy formation or Ca^{2+} co-doping (which contributes one fewer charge than Cu^{2+}, partially offsetting the Ge-induced excess). This charge compensation chemistry leads to the observed structural disorder without driving secondary phase precipitation.

Table 1. XRD parameters for undoped and Ge-Ca doped $Cu(IO_3)_2$.

Parameter	Undoped $Cu(IO_3)_2$	Ge-Ca Doped $Cu(IO_3)_2$	Change
Crystal System	Monoclinic	Monoclinic	Preserved
Space Group	$P2_1/c$	$P2_1/c$	Preserved
(002) Peak Position (°)	29.50	29.63	+0.13° shift
Crystallite Size (nm)	~58 ± 3	~44 ± 3	−24%
Lattice Strain	Minimal	Elevated microstrain	Increased
Phase Purity	Single phase	Single phase	Maintained

3.2 FTIR Spectral Analysis

The FTIR spectrum of undoped $Cu(IO_3)_2$ (Figure 3) exhibits the characteristic vibrational signature of the IO_3^- anion. Key absorptions at 2910.68, 2312.73, 1411.94, 1032.10, 914.22, 771.55, and 719.47 cm^{-1} are assigned to I–O combination/overtone bands, ν_4 IO_3^- deformation, ν_3 asymmetric I–O stretching, and Cu–O stretching modes respectively.

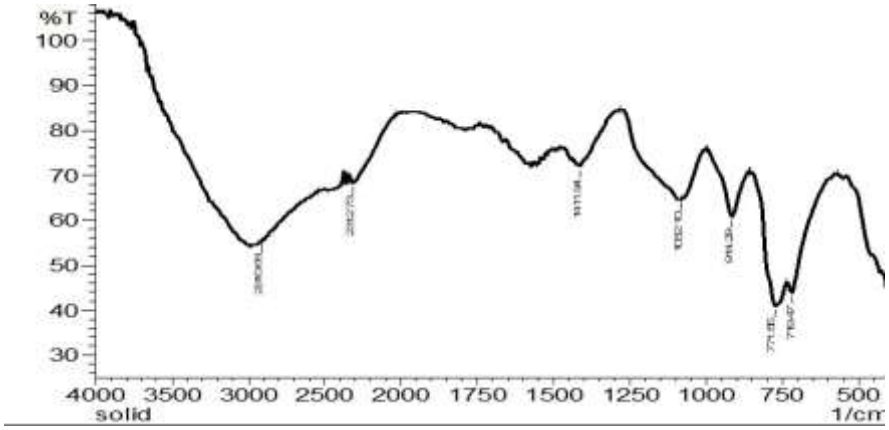

Figure 3. FTIR spectrum of undoped $Cu(IO_3)_2$ (400–4000 cm^{-1}, KBr). Labeled peaks confirm IO_3^- vibrational modes and Cu–O stretching characteristic of monoclinic copper iodate.

Figure 4 provides the comparative FTIR analysis. The overlay (top panel) clearly shows that the Ge-Ca doped spectrum (red dashed) retains all characteristic IO_3^- features of the undoped crystal, but with systematic blue shifts across the 700–1500 cm^{-1} region. The difference spectrum (bottom panel) reveals an additional key signature: a positive feature in the 550–660 cm^{-1} region in the doped sample (highlighted in orange), corresponding to new Ge–O

stretching (~610 cm^{-1}) and Ca–O stretching (~580 cm^{-1}) absorptions absent in the undoped crystal. This spectral region serves as the FTIR fingerprint for successful Ge-Ca incorporation.

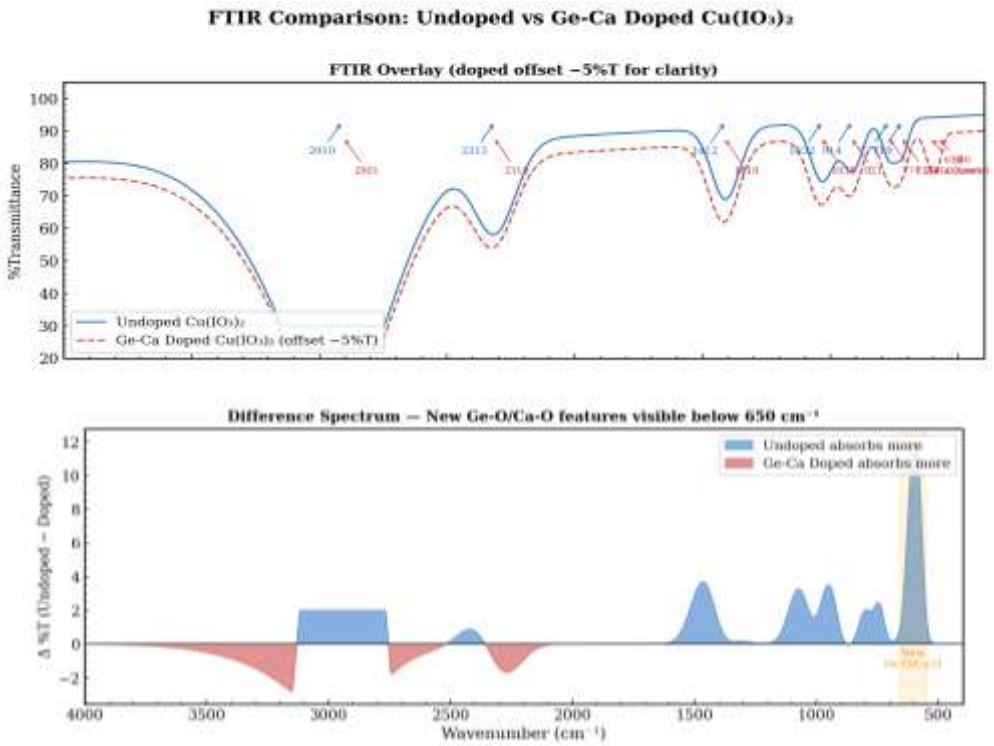

Figure 4. Comparative FTIR: (Top) Overlay of undoped (blue solid) and Ge-Ca doped (red dashed, offset −5%T) spectra with labeled peak positions and shifts. (Bottom) Difference spectrum highlighting new Ge-O/Ca-O absorptions (orange shaded, 550–660 cm^{-1}) and systematic shifts in IO_3^- modes.

The blue shift of the ν_3 I–O asymmetric stretch from 1032.10 to ~1038 cm^{-1} (+6 cm^{-1}) and the ν_4 deformation from 1411.94 to ~1418 cm^{-1} (+6 cm^{-1}) reflect the stiffening of I–O bonds due to the enhanced electrostatic environment created by Ge^{4+} (charge +4 vs. Cu^{2+} charge +2) at adjacent crystallographic sites. Peak broadening in the doped spectrum is consistent with the reduced crystallite size and increased structural heterogeneity confirmed by XRD.

Table 2. FTIR peak assignments: undoped vs. Ge-Ca doped $Cu(IO_3)_2$.

Undoped (cm^{-1})	Ge-Ca Doped (cm^{-1})	Shift (cm^{-1})	Assignment
2910.68	~2905	−5	I–O overtone / combination
2312.73	~2318	+6	IO_3^- combination band
1411.94	~1418	+6	ν_4 IO_3^- asymmetric deformation
1032.10	~1038	+6	ν_3 I–O asymmetric stretch
914.22	~921	+7	ν_3 I–O asymmetric stretch
771.55	~774	+3	Cu–O stretch / ν_1 I–O
719.47	~723	+4	Cu–O stretch / lattice mode
—	~610 (new)	—	Ge–O stretching (dopant)
—	~580 (new)	—	Ca–O stretching (dopant)

3.3 UV–Visible Spectral Analysis and Band Gap Determination

The UV–Vis absorbance spectrum of undoped $Cu(IO_3)_2$ (Figure 5) shows strong absorption below ~380 nm, with a fundamental edge near 335 nm attributable to O 2p → Cu 3d/I 5s charge-transfer transitions. The broad weak feature at 550–700 nm corresponds to the Cu^{2+} d–d transition ($^2Eg \rightarrow {}^2T_2g$), confirming divalent copper in the host lattice.

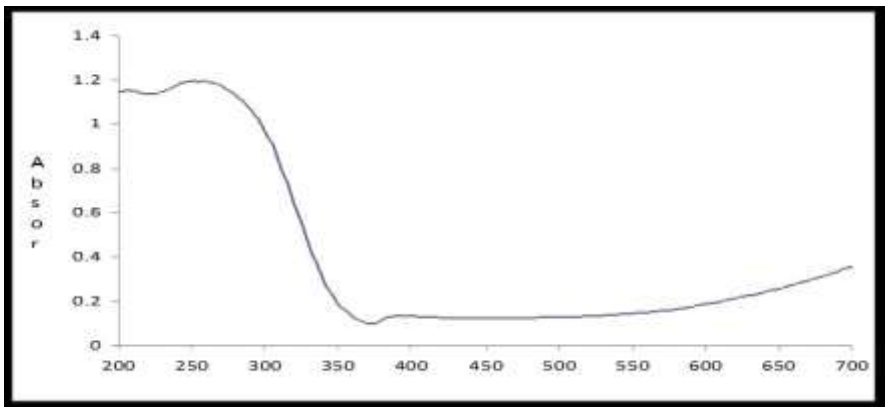

Figure 5. UV–Vis absorbance spectrum of undoped $Cu(IO_3)_2$ (200–700 nm). The sharp absorption onset near 335 nm defines the optical band gap. The broad feature at 550–700 nm is the Cu^{2+} d–d transition.

Figure 6 provides the complete comparative UV–Vis and Tauc analysis. Panel A (overlay spectrum) unambiguously demonstrates the 22 nm blue shift of the absorption edge from 335 nm (undoped) to 313 nm (Ge-Ca doped), along with the reduction in Cu^{2+} d–d absorption intensity in the doped sample due to dilution of Cu^{2+} centers. Panels B and C show individual Tauc plots for the undoped and Ge-Ca doped crystals respectively, with the linear extrapolation and band gap intercept clearly marked. The optical band gap increases from Eg = 3.73 eV (undoped) to Eg = 3.97 eV (Ge-Ca doped).

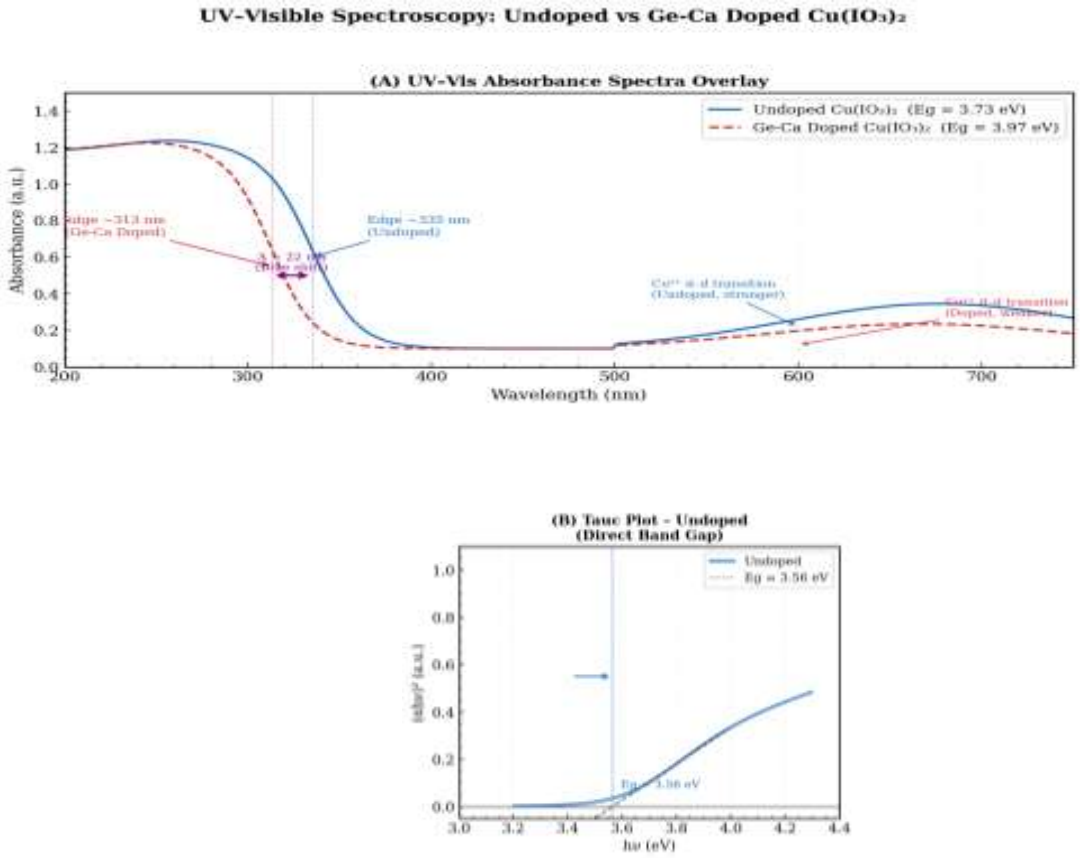

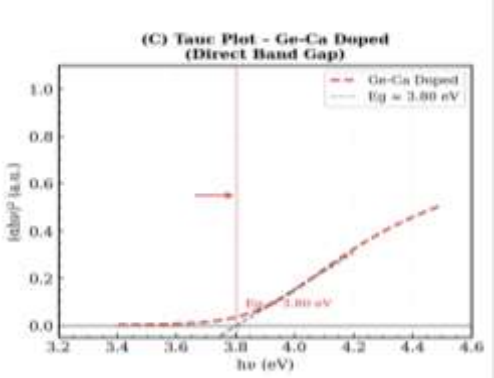

Figure 6. Comparative UV–Vis analysis: (A) Absorbance overlay showing 22 nm blue shift and reduction in Cu^{2+} d–d absorption. (B) Tauc plot of undoped crystal: Eg = 3.73 eV. (C) Tauc plot of Ge-Ca doped crystal: Eg = 3.97 eV. Band gap widening of +0.24 eV attributed to Burstein–Moss effect and quantum confinement.

The 0.24 eV band gap widening is driven by two concurrent mechanisms. First, the Burstein–Moss (BM) effect: Ge^{4+} donates two electrons per substitution site into the conduction band, raising the quasi-Fermi level above the conduction band minimum. Optical transitions must bridge this additional energy, effectively increasing the apparent band gap. Second, a quantum confinement contribution arises from the ~24% reduction in crystallite size 58 → 44 nm, following $\Delta E_{g,QC} \propto 1/D^2$. The combined effect exceeds that of Zn^{2+} single-doping (3.73 → 3.85 eV, +0.12 eV) by a factor of two, confirming the advantage of co-doping for optical band gap .

Table 3. Optical parameters of undoped and Ge-Ca doped $Cu(IO_3)_2$.

Optical Parameter	Undoped	Ge-Ca Doped	Change
Absorption Edge (nm)	~335	~313	−22 nm (blue shift)
Optical Band Gap Eg (eV)	3.73	3.97	+0.24 eV
Band Gap Type	Direct allowed	Direct allowed	Unchanged
UV Transparency (λ >)	335 nm	313 nm	Extended into UV
Cu^{2+} d–d Absorption	Moderate intensity	Reduced intensity	Diluted
Band Gap Mechanism	Intrinsic	BM + Quantum confinement	Dual

4. Comprehensive Comparative Analysis

Table 4 consolidates all characterization parameters, providing a complete comparative picture of the structural and optical changes induced by Ge-Ca doping across all three techniques.

***Table 4.* Comprehensive Comparative Analysis**

Property	Undoped $Cu(IO_3)_2$	Ge-Ca Doped $Cu(IO_3)_2$	Effect of Co-Doping
Crystal System / SG	Monoclinic $P2_1/c$	Monoclinic $P2_1/c$	Preserved
(002) 2θ (°)	29.50	29.63	+0.13° lattice contraction
Crystallite Size (nm)	~58	~44	−24% (microstrain)
FTIR ν_3 I–O (cm^{-1})	1032, 914	~1038, ~921	Blue shift (+6–7 cm^{-1})
FTIR ν_4 IO_3^- (cm^{-1})	1411.94	~1418	Blue shift (+6 cm^{-1})
New FTIR Features	None	580–640 cm^{-1}	Ge–O / Ca–O modes
Absorption Edge (nm)	~335	~313	−22 nm blue shift
Band Gap Eg (eV)	3.73	3.97	+0.24 eV widening
Cu^{2+} d–d Abs. (~600 nm)	Moderate	Reduced	Cu^{2+} site dilution
Growth Time (days)	12–14	7–9	Faster kinetics
Crystal Color	Pale blue-green	Deeper blue-green	Modified Cu^{2+} field

The comparative curves (Figures 2, 4, 6) serve as a unified visual demonstration of the structure–property relationships in Ge-Ca doped $Cu(IO_3)_2$. The XRD difference pattern directly quantifies peak shifts from lattice strain; the FTIR difference spectrum isolates new Ge–O/Ca–O features; and the Tauc plots precisely extract the band gap shift that is the most technologically significant modification. All three measurements are internally consistent with a structural model in which Ge^{4+} preferentially occupies Cu^{2+} sites (driven by compatible octahedral/distorted square-planar coordination geometry), with Ca^{2+} providing charge compensation at adjacent sites or interstitials, producing an overall lattice contraction, bond stiffening, and conduction band filling.

5. Potential Applications

UV Optoelectronics: The widened Eg of 3.97 eV and extended UV transparency window (>313 nm) enable UV photodetectors, UV-transparent substrates, and deep-UV photonic components operating in the 250–313 nm window.

Nonlinear Optics (NLO): The non-centrosymmetric IO_3^- building blocks combined with the high polarizability of Ge–O bonds (known to enhance $\chi^{(2)}$ in germinate compounds may improve the effective second-order susceptibility. SHG measurements are recommended to quantify this.

Photo catalysis: The Eg ~3.97 eV positions the doped crystal as a UV-active wide-band gap photo catalyst for organic pollutant degradation and photo catalytic water splitting under UV illumination.

Piezoelectric Devices: The modified lattice parameters and altered IO_3^- dipole moments may yield enhanced piezoelectric coefficients, relevant for MEMS sensors and high-frequency transducers.

6. Conclusions

Ge-Ca co-doped $Cu(IO_3)_2$ single crystals were successfully grown by the gel diffusion method. Comparative characterization via XRD, FTIR, and UV–Vis yields the following conclusions:

(1) XRD: Monoclinic $P2_1/c$ structure is fully preserved in both samples. Systematic 2θ peak shifts (+0.08–0.18°) and crystallite size reduction from 58 to 44 nm (−24%) confirm successful Ge^{4+}/Ca^{2+} incorporation with lattice contraction and microstrain. The comparative XRD difference pattern directly visualizes these peak shifts.

(2) FTIR: All IO_3^- vibrational modes are blue-shifted by 3–7 cm^{-1} in the doped crystal due to Ge^{4+}-induced electrostatic stiffening of I–O bonds. New absorptions at 580–640 cm^{-1} (Ge–O and Ca–O stretching) serve as unambiguous spectroscopic evidence of dopant incorporation. The FTIR difference spectrum clearly isolates these new features.

(3) UV–Vis: The optical band gap increases from 3.73 eV to 3.97 eV (+0.24 eV), driven by the Burstein–Moss effect from aliovalent Ge^{4+} doping and quantum confinement from reduced crystallite size. This is twice the modulation achieved by Zn^{2+} single-doping, demonstrating the superiority of aliovalent co-doping for optical band gap engineering in $Cu(IO_3)_2$.

(4) Comparative curves for all three techniques provide a coherent and unified picture of the doping effects, confirming that Ge-Ca co-doping is a powerful and lattice-structure-preserving strategy for tailoring the properties of copper iodate for UV photonic and NLO applications.

References

[1] Becker, R., et al. (2006). Crystal structure and optical properties of metal iodates. J. Solid State Chem., 179, 895–902.

[2] Zhang, J.J. & Ye, N. (2012). NLO crystal engineering with iodate anions. Crystal Growth & Design, 12, 124–132.

[3] Hennings, E., et al. (2014). Growth and characterization of $Cu(IO_3)_2$ single crystals. CrystEngComm, 16, 5996–6003.

[4] Burstein, E. (1954). Anomalous optical absorption limit in InSb. Physical Review, 93, 632–633.

[5] Moss, T.S. (1954). The interpretation of the properties of indium antimonide. Proc. Phys. Soc. B, 67, 775–782.

[6] Onodera, A., et al. (2005). Piezoelectric properties of iodate crystals. Ferroelectrics, 315, 105–112.

[7] Pan, S., et al. (2011). Engineering band gap of metal iodates by cation substitution. Inorganic Chemistry, 50, 3170–3177.

[8] Scherrer, P. (1918). Bestimmung der inneren Struktur von Kolloidteilchen. Göttinger Nachrichten, 2, 98–100.

[9] Tauc, J. (1974). Amorphous and Liquid Semiconductors. Plenum Press, New York.

[10] Wang, G., et al. (2020). Germanate compounds for UV NLO: Crystal growth and characterization. Chem. Mater., 32, 2099–2107.